JOURNAL OF PROPULSION AND POWER
Vol. 17, No. 3, May–June 2001

Small-Bore Ram Accelerator Operation

A. Sasoh,* Y. Hamate,† and K. Takayama‡
Tohoku University 2-1-1 Katahira, Aoba-ku, Sendai 980-8577, Japan

Experimental study is conducted in a 25-mm-bore ram accelerator at mixture fill pressures of 2.5 and 3.5 MPa. The obturator motion is analytically modeled to understand the effects of perforation ratio and entrance velocity on the drag coefficient and the mixture ignition delay time. The ram acceleration is achieved at both pressures. At 2.5 MPa the starting and operation characteristics are marginal, whereas increasing the pressure to 3.5 MPa results in better starting reliability and ram acceleration characteristics.

Nomenclature

A	=	cross-sectional area
A_1	=	cross-sectional area of tube
a	=	speed of sound
C_d	=	drag coefficient of obturator
C_p	=	specific heat at constant pressure
D	=	drag exerted on obturator
d	=	tube diameter
h	=	enthalpy
M	=	flow Mach number
m	=	mass
p	=	pressure
p_1	=	mixture fill pressure
Q	=	dimensionless heat release (heat release normalized by $C_{p,1}T_1$)
T	=	temperature
t	=	time
U	=	velocity
U_{CJ}	=	Chapman–Jouguet detonation velocity
$U_{o,e}$	=	obturator entry velocity
u	=	particle velocity
X	=	molar number of CH_4 to two mole of O_2
x	=	travel from the entrance of ram acceleration section
Y	=	molar number of N_2 to two mole of O_2
γ	=	specific heat ratio
Δt	=	difference in arrival time from projectile throat to obturator
ρ	=	density of gas
τ_i	=	ignition delay time
τ_m	=	mechanical characteristic time on obturator separation
ϕ	=	obturator perforation ratio
$\{\_\}$	=	quantity on frame of reference attached to shock wave
$\{/\}$	=	quantity on frame of reference attached to obturator

Subscripts

e	=	value at ram accelerator tube entrance
o	=	obturator
p	=	projectile
s	=	shock wave

Introduction

THE ram accelerator is a chemically propelled mass launcher that is characterized by its long effective acceleration period, heavy payload capability, and reasonable scalability.[1] Intensive experimental studies,[2–13] including that described in a private communication with S. Ohyagi in 1997, have been conducted, and ram accelerations have been realized in facilities with bore dimensions from 25 to 120 mm diameter (circular) and 15 × 20 mm (rectangular). Bruckner has reported a ram acceleration of 2.7 km/s in a 38-mm-bore device.[2] This is currently the highest achievable value. However, to realize various applications such as a direct or first-stage space launcher,[14,15] this value is not sufficient.

It is not always possible to build large facilities capable of investigating achievable performance of the ram accelerator. On the other hand, a small device capable of high acceleration is very useful to fundamental studies. In fact, to date, relatively high projectile velocities are obtained in small-bore facilities, such as 2.7 km/s in a 38-mm bore[2] and 2.4 km/s in a 30-mm bore,[16] whereas in large-bore facilities achieved projectile velocities are relatively low, 2.2 km/s in a 90-mm bore[16] and 2.0 km/s in a 120-mm bore.[17] However, operation characteristics of even smaller devices have not been extensively studied. The 25-mm-bore ram accelerator at the Shock Wave Research Center (SWRC) is by far the smallest ram accelerator in the world among currently operational ones. (The ram accelerator of Hiroshima University of a 15 × 20 mm rectangular bore is smaller. However, the operation pressure is limited to 0.5 MPa; it is run mainly for flow visualization, not for investigating the achievable performance features.)

In the ram accelerator operation, a projectile is accelerated in a preaccelerator device, which is either a light-gas gun or a powder gun, up to a velocity high enough to start the ram acceleration. Usually, during the preacceleration, the projectile is backed by a piston having surface perforations, which is commonly referred to as an obturator. The perforations, in turn, are plugged by a backplate during the preaccelerationstage. The obturator acts not only as the plug, but also assists in the mixture ignition through shock heating.[1] In the case of the successful start of the subdetonative mode[1] operation, subsonic combustion is established and sustained. Therefore, the design of the obturator is critical for the success of any ram accelerator. To improve starting reliability, the obturator-associated ignition process needs to be investigated further.

The purpose of the present study is to investigate the operational characteristics of a 25-mm-bore ram accelerator, identifying and discussing features peculiar to a small-bore device, including the obturator-associated ram acceleration starting.

Experimental Apparatus

Figure 1 schematically illustrates the ram accelerator, RAMAC 25, at SWRC used in the present study. It has a 25-mm-bore, 6-m-long ram acceleration section. The fill pressures in the ram acceleration tube, p_1, varies from 2.5 to 3.5 MPa. The passage of the projectile throat (in this paper, the location where the cross-sectional area of the flow passage is smallest is referred to as a throat; this applies both to the projectile and the obturator, see Figs. 2 and 3) is detected by sensing its magnetic induction generated from a rubber ring magnet embedded in the projectile. Pick-up coils are flush

Received 23 October 1999; revision received 11 May 2000; accepted for publication 24 August 2000.

*Associate Professor, Shock Wave Research Center, Institute of Fluid Science. Associate Fellow AIAA.

†Graduate Student, Shock Wave Research Center, Institute of Fluid Science. Student Member AIAA.

‡Professor, Shock Wave Research Center, Institute of Fluid Science. Senior Member AIAA.

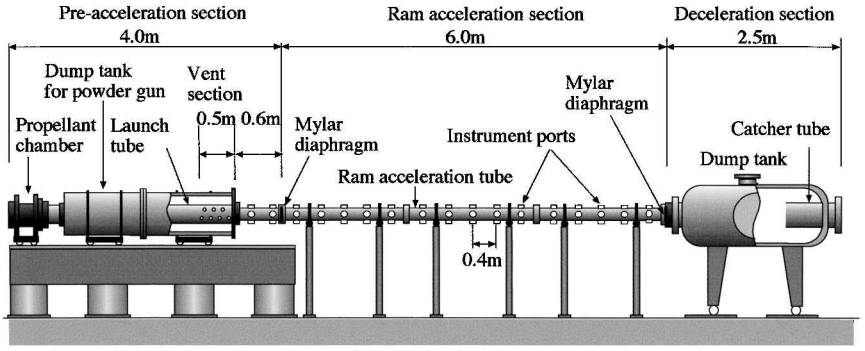

Fig. 1 Schematic of the ram accelerator, RAMAC25.

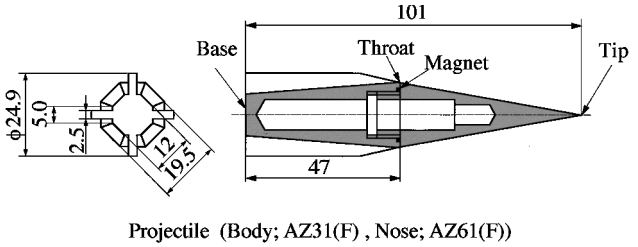

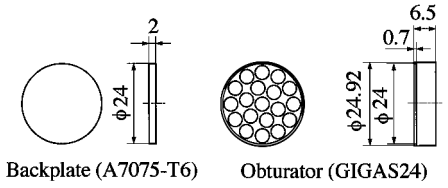

Fig. 2 Projectile, obturator, and backplate.

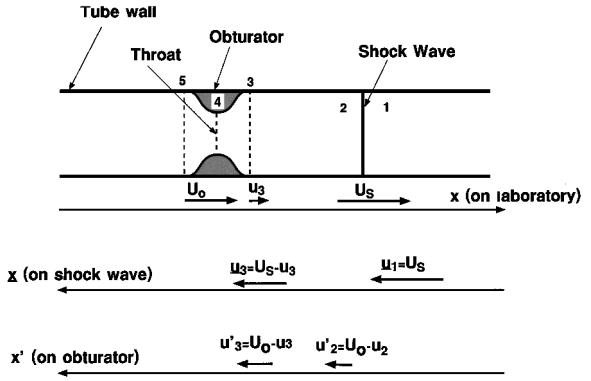

Fig. 3 Model of obturator-associated flow and frames of reference used in the analysis.

mounted on the inner wall of the ram acceleration tube. The axial separation distance between adjacent coils is around 0.4 m. In addition, piezoelectric pressure transducers with typical rise time of 1 μs are flush mounted at an angle of 90 deg from the axis of the coil.

The configurations of the projectile, obturator, and backplate are shown in Fig. 2. The projectile comprises a hollow conical nose (half-apex angle of 10 deg) threaded to a body. To reduce the mass, both the conical nose and the body comprising four fins are fabricated using magnesium alloy [nose, AZ61(f); body, AZ31(F)].

The obturator is fabricated using a newly developed aluminum alloy, GIGAS24 or GIGAS30 (tensile stress of 700 MPa at room temperature and density of $\sim 3.0 \times 10^3$ kg/m^3, YKK Cooperation). The perforation ratio of the obturator, $\phi = 0.54$, achieved in the present study, is mainly attributed to the high specific strength of the material. Experiments are also carried out using magnesium alloy AZ31(F) obturators. However, the backplate is made of aluminum alloy, A7075-T6, in this study. The projectile backed by the obturator and backplate is launched using a powder gun charged with an up to 26-grams single-base smokeless powder (NY500, Nippon Oil and Fats Cooperation).

Methane, oxygen, and nitrogen are individually supplied using the respective mass flow controllers and are mixed together at the inlet of a 35-m-long feed tube, which, in turn, connects to the ram acceleration tube. The pressure difference between the inlet and outlet of each mass flow controller is regulated using a back-pressure regulator installed on its outlet side.

The measured signals are recorded in a data acquisition system and are processed using a personal computer. Further details of the experimental apparatus have been explained elsewhere.[8,10]

Obturator Separation Model

In the preaccelerator, a projectile and an obturator are accelerated together up to an entrance Mach number over 3.0. The function of the obturator is not only to plug the driver gas, but also to generate a shock-compressed gas slug after entering the ram acceleration tube. During ignition of the mixture, the obturator is strongly decelerated and eventually does not affect the flowfield around the projectile. Whether or not the ram acceleration is successfully accomplished depends strongly on the obturator-associated mixture ignition process.

Precursory shock waves generated by an obturator in the preaccelerator launch tube have been studied by Burnham,[18] Stewart et al.,[19] and Sasoh et al.[20] In an earlier study carried out jointly by the University of Washington and the French–German Research Institute at Saint Louis,[21,22] detonation initiation either by the direct impact of a piston (solid obturator) or by a transmitting detonation wave generated by the piston have been investigated. Under low pressures, the initiated detonation is only marginal. Recently, Schultz et al.[23,24] have systematically determined the ignition conditions of ram accelerator mixtures using a solid/perforated obturator with/without a projectile. The measured motions of the solid obturator are compared with a numerical computation using the method of characteristics. However, it is very essential to analyze quantitatively the effects of perforation on the obturator motion and mixture ignition.

Against this backdrop, an analytical model has been developed to understand the sensitivity of the obturator design to the ram acceleration starting precess. Here, the following assumptions have been made:

1) The process is quasi steady.

2) The effect of projectile on the obturator is neglected (the obturator motion is determined by the mixture interaction with the movement of obturator).

3) The backplate comes off from the obturator and disappear when the obturator enters the ram acceleration tube.

4) The heat release of combustion is neglected.

A normal shock wave driven by a right-running obturator with passage area contraction for the gas is shown in Fig. 3. The cross-sectional area ratio of the obturator throat (label 4) to the tube (label 1) is referred to as a perforation ratio ϕ, which is given by

$$\phi \equiv A_4 / A_1 \tag{1}$$

A streamline is assumed to go along the smooth inner surface of the obturator. Here, three frames of reference are defined: An axial

coordinate on the frame of reference fixed on the laboratory is designated as x; those on the shock wave and on the obturator are represented as $\underline{x}$ and x', respectively. Under the assumption of a quasi steady state, Galilean transformation is applicable among motions expressed in these frames of reference. The origin of the x coordinate is at the entrance of the ram acceleration tube. The velocities of the shock wave and the obturator measured on the frame of reference attached to the laboratory are designated by U_s and U_o, respectively. The particle velocities on the frames of reference attached to the laboratory, the shock wave, and the obturator are designated by u, $\underline{u}$, and u', respectively. The quiescent state in front of the shock wave is labeled by 1. Label 2 represents the postshock state. Labels 3–5 sequentially represent the states at the inlet, throat, and outlet of the obturator, respectively. Without chemical reaction, quantities do not vary between at states 2 and 3. At state 3, the flow is subsonic with respect to the obturator, at state 5 it is supersonic. A choking condition is applied to the state 4.

Applying Rankine–Hugoniot relations in the frame of reference attached to the shock wave between the states 1 and 3, we get

$$\rho_1 \underline{u}_1 = \rho_3 \underline{u}_3 \tag{2}$$

$$\rho_1 \underline{u}_1^2 + p_1 = \rho_3 \underline{u}_3^2 + p_3 \tag{3}$$

$$h_1 + \tfrac{1}{2}\underline{u}_1^2 = h_3 + \tfrac{1}{2}\underline{u}_3^2 \tag{4}$$

where h represents static enthalpy.

Isentropic relations for calorically perfect gas (constant γ) are applied to the flow from state 3 to 5. On the frame of reference attached to the obturator, the relations can be expressed as

$$\frac{A}{A_1} = \frac{M_3'}{M'} \left\{ \frac{1 + [(\gamma - 1)/2]M'^2}{1 + [(\gamma - 1)/2]M_3'^2} \right\}^{(\gamma+1)/2(\gamma-1)} \tag{5}$$

$$\frac{p}{p_3} = \left\{ \frac{1 + [(\gamma - 1)/2]M_3'^2}{1 + [(\gamma - 1)/2]M'^2} \right\}^{\gamma/(\gamma-1)} \tag{6}$$

$$M_3' = \frac{U_o - U_s + \underline{u}_3}{a_3} \tag{7}$$

Then the drag force experienced by the obturator D is given by

$$D = -\int_3^5 p \, \mathrm{d}A \tag{8}$$

For evaluating the drag force, the appropriate reference value is calculated from the mixture fill pressure p_1. Therefore, the drag coefficient C_d is defined as

$$C_d \equiv D / p_1 A_1 \tag{9}$$

Figure 4a shows contours of C_d for a given mixture used in the study. C_d sharply decreases as a function of ϕ, but slightly increases with increasing U_o. For a constant thickness and material density, the mass of an obturator is in proportion to $1 - \phi$ (in practical experiments, an obturator has rim to hold a backplate that causes a small deviation from this proportionality). In determining the deceleration of the obturator, these two effects compete with each other. The deceleration scales with $C_d/(1 - \phi)$. As seen in Fig. 4b, $C_d/(1 - \phi)$ is still a sharply decreasing function of ϕ. The higher ϕ, the more slowly the obturator separates from the projectile. It is observed that $C_d/(1 - \phi)$ is more sensitive to U_o than C_d.

With Eqs. (2–8) used, the motions of the obturator can be calculated numerically by integrating its equation of motion with respect to time. In the calculation, the shock speed, $U_s = \underline{u}_1$, is determined to match the choking condition at state 4. Typical x–t diagrams of obturator motion are shown in Fig. 5. The operation conditions coincide to those of the case C in Fig. 6a. As a reference, the trajectory of the projectile at the constant velocity is also plotted. If the passage time is monitored at $x = 0.20$ m, the delay time of the obturator passage to the projectile throat will be 60 μs. As will be shown later, this value is fairly close to the measured one.

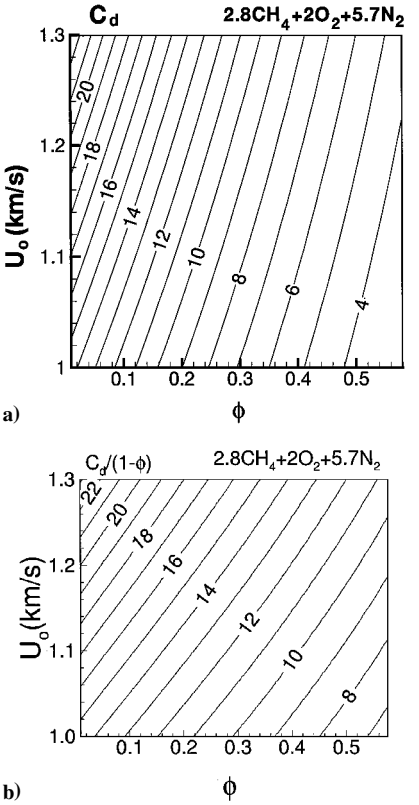

Fig. 4 Contours of constant value of a) C_d and b) $C_d/(1 - \phi)$ on ϕ–U_o coordinates, T_1 = 288.15 K.

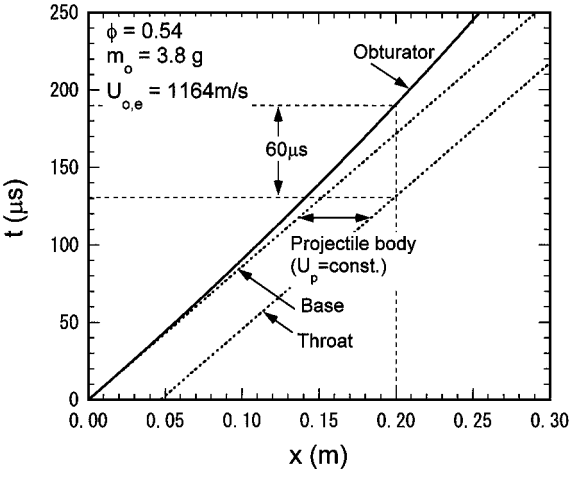

Fig. 5 Example of x–t diagram of obturator trajectory; trajectory of the projectile at a constant speed is also plotted.

Results and Discussion

Obturator-Associated Ram Acceleration Start

Table 1 shows the typical experimental conditions of the present study. Here, a quantity at the entrance of the ram acceleration tube is designated with a subscript e. In the present study, the tube wall pressure histories at $t = 0$ correspond to the passage time of the projectile throat. Figures 6a and 6b show the pressure histories measured near the entrance of the ram acceleration section using three different obturators with different perforation ratios ϕ. The obturator arrival is indicated by a pressure drop; for example, at $\Delta t = 60$ μs for the case C. Also, the arrival times of the obturator front calculated using the analytical model described in the preceding section (see Fig. 5) are plotted. As seen in Fig. 6a, the calculated arrival times quantitatively agree with the respective experimental results.

In cases A and B, the obturator material is magnesium alloy, whereas in case C, GIGAS is used. Although the mass does not vary

Table 1 Conditions of experiment

Case	p_1, MPa	$U_{o,e}$, m/s	ϕ	m_o, grams	Result[a]	Comment
A	2.5	1183	0.37	3.3	US	Small perforation
B	2.5	1185	0.46	2.8	RA	Medium perforation
C	2.5	1164	0.54	3.8	RA	Large perforation
D	2.5	1206	0.46	4.1	RA	Heavy obturator
E	2.5	1124	0.46	2.8	WF	Low velocity
F	3.5	1182	0.54	3.7	RA	High pressure

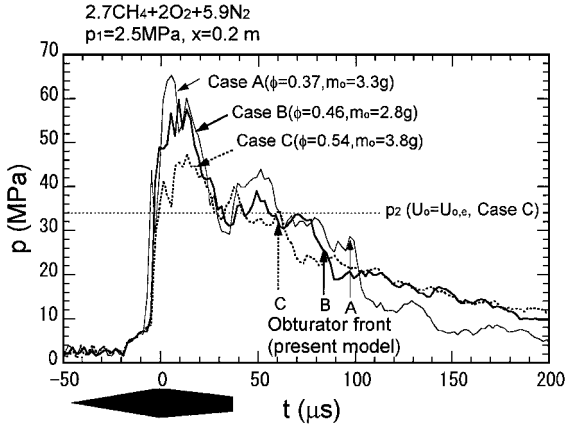

a) $x = 0.20$ m

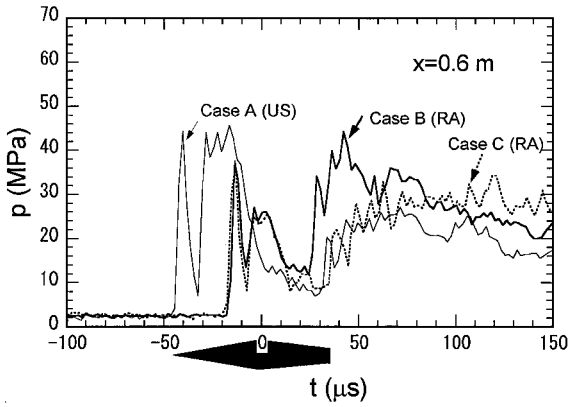

b) $x = 0.60$ m

Fig. 6 Time variations of tube wall pressure with three different obturators, p_1 = 2.5 MPa and 2.7CH4 + 2O2 + 5.9N2.

linearly with ϕ, the pressure histories represent the effect of ϕ on the obturator dynamics: In case A, with the lowest ϕ, the obturator arrives at the location last because of the highest deceleration. Because the obturator-driven shock wave is strongest, the mixture ignition progresses considerably at the location; the peak pressure is highest. The additional pressure spike of sonic diffuser unstart[24,25] (US) in Fig. 6b implies that the shock wave is ahead of the projectile throat. In cases B and C, ram acceleration (RA) is successfully started.

Figure 7a shows the pressure histories measured with obturators having different masses. The analytically calculated obturator trajectories are shown in Fig. 7b. In both cases, the measured obturator arrival time agrees well with the calculated value.

In Figs. 8a and 8b, pressure histories measured at different entrance velocities $U_{o,e}$ are plotted. In Fig. 8a, Δt is calculated using the present model and agrees well with the experimental results. In case E, $U_{o,e}$ is not high enough to generate a strong shock wave to ignite the mixture during the obturator separation process. The pressure history at $x = 0.6$ m (Fig. 8b) exhibits wave fall-off[24,25] (WF), which means that the projectile is not driven by a combustion-driven shock wave but supersonically coasts in the tube.

Figure 9 shows a pressure history measured at $x = 0.236$ m with a higher fill pressure, $p_1 = 3.5$ MPa (case F). The calculated obturator arrival time agrees well with the measured value. However, the measured pressure level is lower than p_2 estimated from $U_{o,e}$.

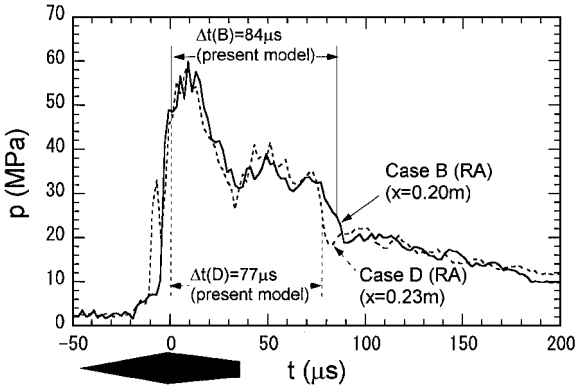

Fig. 7a Time variation of tube wall pressure with different obturator masses, p_1 = 2.5 MPa, 2.7CH4 + 2O2 + 5.9N2, and ϕ = 0.46.

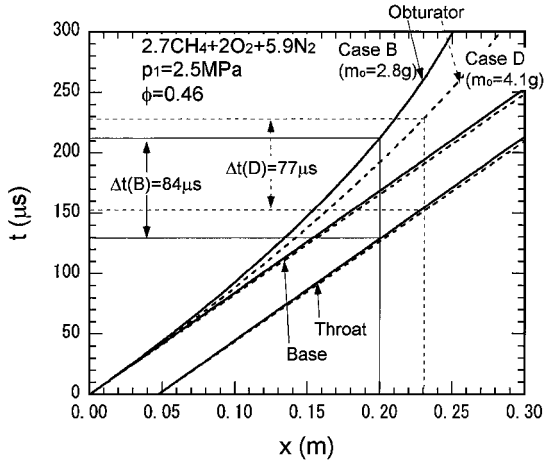

Fig. 7b Obturator trajectory x–t diagrams under the corresponding operation conditions.

At higher fill pressures, the obturator decelerates faster, leading to a substantial pressure decrease before significant heat release. In cases C and F, only the fill pressures are different. In case C (in Fig. 6a) (lower fill pressure), the mixture ignition gets progressed even at $x = 0.20$ m; the measured pressure exceeds p_2 estimated from $U_{o,e}$.

Starting Characteristics

The results show that the analytical model can be used to accurately calculate the obturator motion, which helps in better understanding the experimental results. The question is how to apply the model to RA starting characteristics observed in the facilities of different dimensions.

A mechanical characteristic time τ_m, during which, with a constant drag D_e, the obturator becomes separated from the projectile base by a distance d, is calculated by

$$\tau_m \equiv (2dm_o/D_e)^{\frac{1}{2}} = \tau_m(U_{o,e}, \phi, p_1, m_o, d) \tag{10}$$

The ignition delay time τ_i is a function of the following parameters:

$$\tau_i = \tau_i(T_1, p_1) = \tau_i(U_{o,e}, \phi, p_1) \tag{11}$$

In this study, τ_i is given from the Petersen et al. formula presented in Ref. 26.

In Table 2, specifications of obturator design in the 25-mm-bore (present study), the 38-mm-bore [University of Washington (UW)[23,27]], and the 120-mm-bore [Army Research Laboratory (ARL)[4,17,28–30] devices are tabulated. In the present study, polycarbonate cannot be used as the obturator material because with perforation it does not withstand the initial impact of the powder gun in the preacceleration section. An obturator made of magnesium alloy AZ61(F) can be used for $\phi \leq 0.46$. An obturator made of GISAS can attain $\phi = 0.54$.

Results of a ram accelerator starting obtained in the three facilities are summarized in Fig. 10. Although this map does not

Table 2 Obturator specifications under typical operation conditions

Organization	Material	$U_{o,e}$, km/s	ϕ	m_o, kg	p_1, MPa	d, mm	C_d	X	Y
Present study	AZ61(F)	1.18	0.46	2.8×10^{-3}	2.5	25	5.8	2.7	5.9
Present study	GIGAS30	1.18	0.54	3.8×10^{-3}	2.5	25	4.4	2.7	5.9
Present study	GIGAS30	1.18	0.54	3.8×10^{-3}	3.5	25	4.3	2.8	5.7
UW[23]	Polycarbonate	1.15	0.47	1.17×10^{-2}	2.5–5.0	38	5.6	2.8	5.7
ARL[4]	A7075-T6	1.18	0	5.11×10^{-1}	5.1–10.2	120	20	3	10

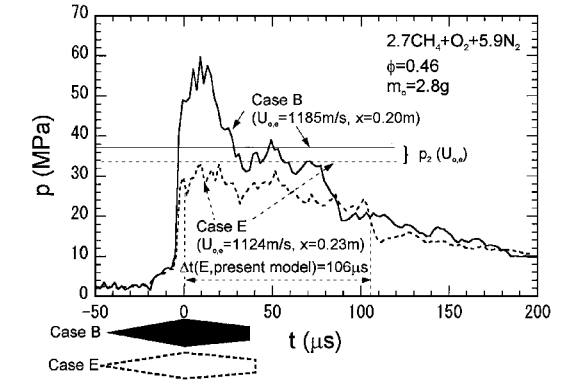

a) $x = 0.20$ m

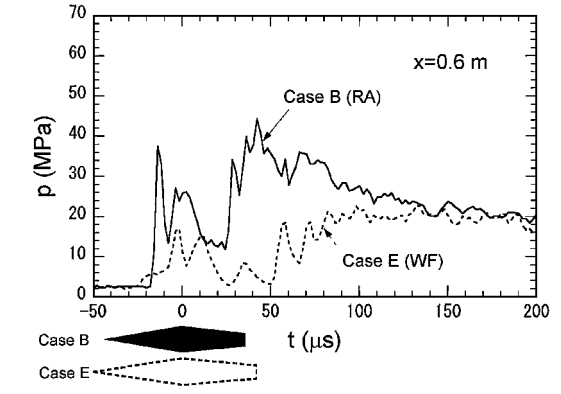

b) $x = 0.60$ m

Fig. 8 Time variations of tube wall pressure with different $U_{o,e}$; p_1 = 2.5 MPa and $2.7CH_4 + 2O_2 + 5.9N_2$.

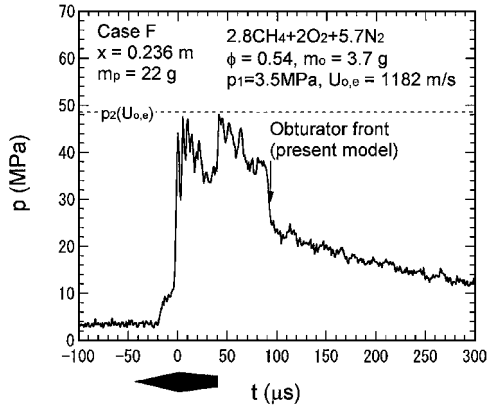

Fig. 9 Time variations of tube wall pressure for p_1 = 3.5 MPa, $2.8CH_4 + 2O_2 + 5.7N_2$, and $x = 0.236$ m.

provide any criterion for successful RA, some indication is evident. With an increase in bore diameter, τ_i / τ_m tends to decrease. In the present study, starting conditions are mapped around $\tau_i / \tau_m \simeq 1$. In the case of UW (38-mm bore), $0.3 < \tau_i / \tau_m \simeq < 1$; in the case of ARL (120-mm bore), $\tau_i / \tau_m < 0.1$. This tendency implies that with increasing bore diameter the mixture ignition is advanced. The combustion-driven shock wave has a complicated front shape and fluctuations. If a projectile body is long enough, the allowance for

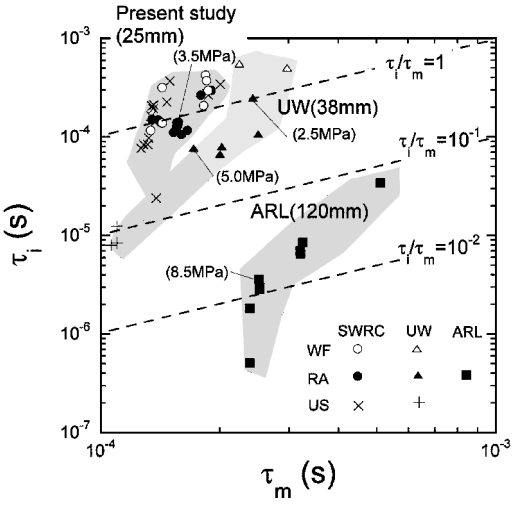

Fig. 10 Starting result map in τ_m vs τ_i coordinates.

a combustion-driven shock wave to stay along the body becomes larger. With a small bore, the allowance becomes smaller, and the margin for the obturator-associated starting reduces appreciably.

In the present study, tendencies exist where τ_i of WF is larger than that of RA and where τ_m of US is smaller than that of RA. However, RA, WF, and US regions cannot be clearly separated. For the small bore of the present study, a margin for the RA starting is considerably small. In the case of UW, although the number of plotted data is limited, a starting regime is better identified.

Advantages and Limitations of the Model

Through the present model, the effect of perforation on the obturator-associated RA starting can be quantitatively addressed. The calculated obturator motion agrees well with the experimental results. In the $\tau_m - \tau_i$ plane, the starting conditions obtained in different facilities are well identified.

However, the present model has some limitations: First, it is applicable only to the beginning stage of the ram accelerator starting because the heat release of the combustion is neglected. Second, because the interaction between the obturator-driven shock wave and the projectile is not taken into account, a definite starting criterion cannot be obtained. Third, because unsteady terms are neglected, the obturator motion can be calculated only when the shock wave is close enough for the assumption of uniform pressure distribution to be applicable for accurate solutions. Further work is mandatory to further improve the model.

RA Characteristics

In this study, RA operation is achieved using methane-fueled mixtures at fill pressures both of 2.5 and 3.5 MPa. Detailed mixture calibration shows slightly different molar ratios for the mixture components in operations at the respective fill pressures. However, as is seen in Table 3, characteristics of these two mixtures are reasonably close. Hence, the effect of these slight differences in the molar ratios can be neglected.

In Fig. 11, measured projectile velocity profiles are plotted. At a fill pressure of 2.5 MPa (closed triangles), the RA is achieved in four shots out of nine. In the case of successful start (case C) near the exit of the ram acceleration tube, U_p slightly exceeded the

Table 3 Characteristics of mixtures used in this study, $XCH_4 + 2O_2 + YN_2$, errors are better than 1%

p_1, MPa	X	Y	a_1, m/s	γ_1	U_{CJ} m/s	Q_{CJ}
2.5	2.7	5.9	357	1.37	1694	4.79
3.5	2.8	5.7	358	1.37	1690	4.73

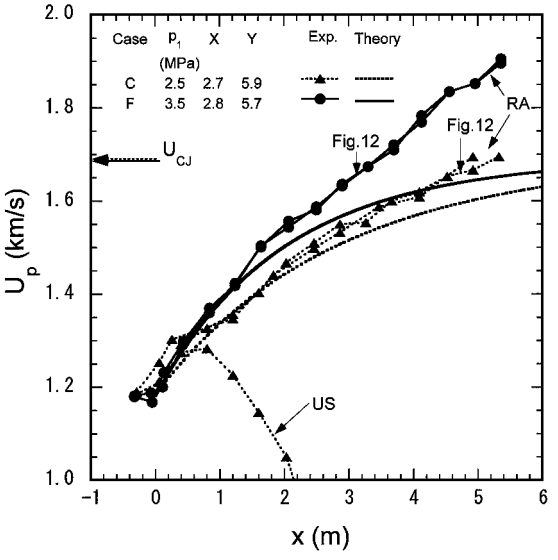

Fig. 11 U_p–x profiles.

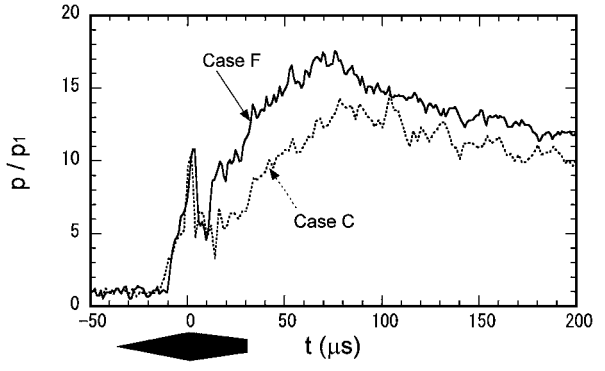

Fig. 12 Time variations of tube wall pressure normalized by the corresponding fill pressure at U_p = 1660 m/s ± 5 m/s.

Chapman–Jouguet detonation velocity U_{CJ}, calculated for an ideal gas. In other cases, sonic diffuser US occurred.

Closed circles denote U_p profiles at higher fill pressure (3.5 MPa, case F). At this fill pressure, the RA is achieved in all seven shots. In these cases, U_p exceeds U_{CJ} and reaches 1.90 km/s. In both cases, the velocity profile agrees well with calculations using the thermally choked Hugoniot relations[31–34] up to about 80% of U_{CJ}. Beyond this value, the measured velocities deviate from the theoretical ones, eventually exceeding U_{CJ}.

Figures 12 show time variations of tube wall pressures p_1 normalized with a fill pressure, measured during the RA operation in cases C and F at a constant U_p (= 1660 m/s ± 5 m/s). Upstream of the throat, the pressure profiles are almost similar to each other. However, the pressure around the projectile body differs. In case C, the pressure around the body is relatively low. A small pressure jump appears at an axial location near the base. In case F, a large pressure jump appears near the throat (at $t = 12$ μs), maintaining the pressure around the body at a higher level. These pressure distributions are well reflected in the projectile accelerations. From Fig. 11, the corresponding thrust coefficients, $C_t = m_p a_p/(p_1 A_1)$, amount to 1 and 2 in cases C and F, respectively, whereas from the thermally choked Hugoniot relation a thrust coefficient at $U_p = 1.66$ km/s in these cases ranges from 0.32 to 0.34. Therefore, in these operations, the measured thrust coefficients are higher than those calculated from the thermally choked Hugoniot relation. Such thrust characteristics are also observed in the 38-mm-bore facility at UW.[34,35] This can be due to the so-called transdetonative operation[34,36] in which the flow is choked on the body and supersonically expands downstream, enhancing the thrust coefficient. Another possible reason is the burning of the magnesium alloy body.[7] However, the real cause has not been well distinguished and still remains unclear. In any case, considerable increase in thrust is achieved during the operation.

Operational Characteristics

Operation at $p_1 = 2.5$ MPa is only marginal; under typical experimental conditions, uncertainty is 5:9. (in Fig. 11, a velocity profile for $p_1 = 2.5$ MPa in the case of wave unstar (US) is also plotted). On the other hand, the operation at $p_1 = 3.5$ MPa is reliable; RA is always realized.

This tendency can be confirmed by observing the measured tube wall pressures. Figures 13a and 13b show measured tube wall pressure histories in case F ($p_1 = 3.5$ MPa) and in case C ($p_1 = 2.5$ MPa), respectively. The passage times of the tip, throat, and base of the projectile are plotted by broken lines. In case F (Fig. 13a), for higher fill pressure, the pressure variations resemble typical ram accelerator operation.[1,32] The pressure spike of the second reflection becomes lower than the peak value, which appears behind the throat. Around the body, a combustion-driven nearly normal shock wave is attached, thereby generating a positive net force to the projectile, that is, thrust.

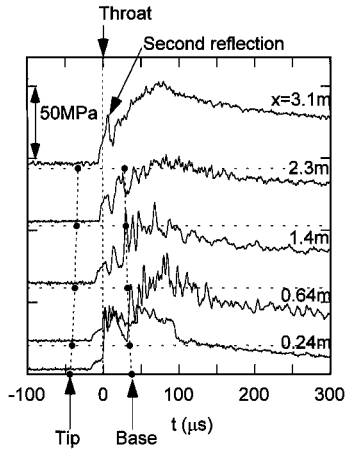

a) p_1 = 2.5 MPa (case C)

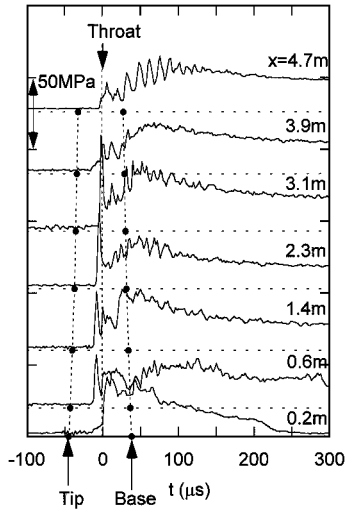

b) p_1 = 3.5 MPa (case F)

Fig. 13 Time variations of tube wall pressures.

In case C (Fig. 13b), a large pressure spike often appears even upstream of the throat. Its peak value fluctuates, being sometimes reasonably low. However, it often exceeds the value corresponding to the combustion-driven shock wave behind the throat. Such a pressure spike can appear due to orientation of the projectile; if a projectile fin is close to the pressure transducer head, profiles of a normal shock wave in front of the fin appear in the measured pressure history.[33] However, in the present experiment this does not seem to be the case. With $p_1 = 2.5$ MPa this pressure spike always appeared, even in such successful RA operation experiments as those of Fig. 13b. With $p_1 = 3.5$ MPa, such a large pressure spike never appeared. If such a peak pressure spike is uniformly distributed all around, then a normal shock wave should propagate upstream, resulting in the wave unstart.[24] However, in these cases, once RA starts, the projectile is accelerated up to the exit of the 6-m-long RA tube. The reasons for such a large pressure spike need to be investigated further.

Conclusions

RA operations have been achieved in the small-bore ram accelerator at fill pressures of 2.5 and 3.5 MPa. The observed RA starting process is analyzed using the present obturator-associated ignition model. The mixture ignition performance is sensitive to the obturator perforation ratio and the obturator velocity. In the experiments, the perforation ratio is increased up to 0.54, resulting in better starting reliability. Through the present work, the scalability of the ram accelerator down to a 25-mm bore has been experimentally verified. However, operation with $p_1 = 2.5$ MPa is only marginal, even after RA starts, whereas it is satisfactory at $p_1 = 3.5$ MPa.

Acknowledgments

The authors acknowledge the kind gesture from YKK Cooperation who provided the newly developed aluminum alloy, GIGAS series for fabricating the obturators. We are grateful to technical support from O. Onodera, H. Ojima, T. Ogawa and M. Adachi of Shock Wave Research Center. Our thanks to M. Kato, K. Asano and K. Takahashi from the machine shop of Institute of Fluid Science for manufacturing the projectiles and related items. The authors would like to thank valuable suggestions and help on various aspects of the present work to A. Hertzberg, A. P. Bruckner, and C. Knowlen of the University of Washington. We acknowledge G. Jagadeesh of the Shock Wave Research Center for valuable discussions and his proofreading the paper.

References

[1]Hertzberg, A., Bruckner, A. P., and Bogdanoff, D. W., "Ram Accelerator: A New Chemical Method for Accelerating Projectiles to Ultrahigh Velocities," *AIAA Journal*, Vol. 26, No. 2, 1988, pp. 195–203.

[2]Bruckner, A. P., "The Ram Accelerator: Overview and State of the Art," *Ram Accelerators*, Springer-Verlag, Heidelberg, Germany, 1998, pp. 3–23.

[3]Bruckner, A. P., Knowlen, C., Hertzberg, A., and Bogdanoff, D. W., "Operational Characteristics of the Thermally Choked Ram Accelerator," *Journal of Propulsion and Power*, Vol. 7, No. 5, 1991, pp. 828–836.

[4]Kruczynski, D. L., "High Performance Ram Accelerator Research," *Ram Accelerators*, Springer-Verlag, Heidelberg, Germany, 1998, pp. 97–104.

[5]Kruczynski, D. L., Horst, A. W., and Liberatore, F., "Experiments in a 120-mm Ram Accelerator at Elevated Pressures," Army Research Lab., Rept. ARL-TR-1236, Aberdeen, MD, 1996.

[6]Giraud, M., Legendre, J. F., and Henner, M., "RAMAC in Subdetonative Propulsion Mode—State of the ISL Studies," *Ram Accelerators*, Springer-Verlag, Heidelberg, Germany, 1998, pp. 65–77.

[7]Seiler, F., Patz, G., Smeets, G., and Srulijes, J., "Presentation of the Rail Tube Version II of ISL's RAMAC 30," *Ram Accelerators*, Springer-Verlag, Heidelberg, Germany, 1998, pp. 79–87.

[8]Sasoh, A., Hirakata, S., Maemura, J., Hamate, Y., and Takayama, K., "Thermally Choked Operation in a 25-mm-Bore Ram Accelerator," *Ram Accelerators*, Springer-Verlag, Heidelberg, 1998, Germany, pp. 111–118.

[9]Sasoh, A., Hirakata, S., Ujigawa, Y., and Takayama, K., "Operation Tests of a 25-mm-Bore Ram Accelerator," AIAA Paper 96-2677, 1996.

[10]Sasoh, A., Hamate, Y., and Takayama, K., "Significance of Unsteadiness in Operation of the Small-Bore Ram Accelerator," AIAA Paper 98-3446, 1998.

[11]Sasoh, A., Hamate, Y., Utsunomiya, G., and Takayama, K., "High Acceleration Ram Accelerator Operations," AIAA Paper 99-2262, 1999.

[12]Chang, X., Matsuoka, S., Watanabe, T., and Taki, S., "Ignition Study for Low Pressure Combustible Mixture in a Ram Accelerator," *Ram Accelerators*, Springer-Verlag, Heidelberg, Germany, 1998, pp. 105–109.

[13]Liu, S., Bai, Z. Y., Jian, H. X., Ping, X. H., and Bu, S. Q., "37-mm Bore Ram Accelerator of CARDC," *Ram Accelerators*, Springer-Verlag, Heidelberg, Germany, 1998, pp. 119–122.

[14]Bruckner, A. P., and Hertzberg, A., "Ram Accelerator Direct Launch System for Space Cargo," International Astronautical Federation, IAF-87-211, 1987.

[15]Kaloupis, P., and Bruckner, A. P., "The Ram Accelerator: A Chemically Driven Mass Launcher," AIAA Paper 88-2968, 1988.

[16]Legendre, J.-F., and Giraud, M., "Enhanced RAMAC Performances in Subdetonative Propulsion Mode With Semi-Combustible Projectile," Paper EF3, Univ. of Poitiers, France, Sept. 1999.

[17]Kruczynski, D. L., "Experimental Investigation of High Pressure/Performance Ram Accelerator Operation," AIAA Paper 96-2676, 1996.

[18]Burnham, E., "Investigation of Starting and Ignition Transients in the Thermally Choked Ram Accelerator," Ph.D. Dissertation, Dept. of Aeronautics and Astronautics, Univ. of Washington, Seattle, WA, Dec. 1993.

[19]Stewart, J. F., Bruckner, A. P., and Knowlen, C., "Effects of Launch Tube Shock Dynamics on Initiation of Ram Accelerator Operation," *Ram Accelerators*, Springer-Verlag, Heidelberg, Germany, 1998, pp. 181–188.

[20]Sasoh, A., Maemura, J., Hirakata, S., Takayama, K., and Falcovitz, J., "Diaphragm Rupture. Impingement by a Conically-Nosed, Ram-Accelerator Projectile," *Shock Waves*, Vol. 9, No. 1, 1999, pp. 19–30.

[21]Bauer, P., Knowlen, C., Higgins, A. J., and Legendre, J. F., "Detonation Initiation of Insensitive Dense Gaseous Mixtures by Piston Impact," *Proceedings of 21st International Symposium on Shock Waves*, Vol. 1, Panther Publ. & Printing, ACT, Australia, 1997, pp. 325–329.

[22]Bauer, P., Legendre, J. F., Knowlen, C., and Higgins, A. J., "A Review of Detonation Initiation Technique for Insensitive Dense Methane–Oxygen–Nitrogen Mixtures," *European Physics Journal, Applied Physics*, Vol. 2, 1998, pp. 183–188.

[23]Schultz, E., Knowlen, C., and Bruckner, A. P., "Overview of the Subdetonative Ram Accelerator Starting Process," *Ram Accelerators*, Springer–Verlag, Heidelberg, 1998, Germany, pp. 189–203.

[24]Schultz, E., Knowlen, C., and Bruckner, A. P., "Obturator and Detonation Experiments in the Subdetonative Ram Accelerator," *Shock Waves*, Vol. 9, No. 3, 1999, pp. 181–191.

[25]Higgins, A. J., Knowlen, C., and Bruckner, A. P., "Ram Accelerator Operation Limits, Part 1: Identification of Limits," *Journal of Propulsion and Power*, Vol. 14, No. 6, 1998, pp. 951–958.

[26]Petersen, E. L., Davidson, D. F., and Hanson, R. K., "Ignition Delay Times of Ram Accelerator CH_4/O_2/Diluent Mixtures, *Journal of Propulsion and Power*, Vol. 15, No. 1, 1999, pp. 82–91.

[27]Schultz, E., "The Subdetonative Ram Accelerator Starting Process," M.S. Thesis, Dept. of Aeronautics and Astronautics, Univ. of Washington, Seattle, WA, March 1997.

[28]Kruczynski, D. L., "New Experiments in a 120-mm Ram Accelerator at High Pressures," AIAA Paper 93-2589, 1993.

[29]Kruczynski, D. L., Liberatore, F., and Kiwan, M., "Flow Visualization of Steady and Transient Combustion in a 120-mm Ram Accelerator," AIAA Paper 94-3344, 1994.

[30]Kruczynski, D. L., "Ram Accelerator Experiments with Unique Projectile Geometries," AIAA Paper 95-2490, 1995.

[31]Knowlen, C., and Bruckner, A. P., "Hugoniot Analysis of the Ram Accelerator," *Shock Waves, Proceedings of the 18th International Symposium on Shock Waves*, Springer-Verlag, Heidelberg, Germany, 1992, pp. 617–622.

[32]Bruckner, A. P., Knowlen, C., Hertzberg, A., and Bogdanoff, D. W., "Operational Characteristics of the Thermally Choked Ram Accelerator," *Journal of Propulsion and Power*, Vol. 7, No. 5, 1991, pp. 828–836.

[33]Hinkey, J. B., Burnham, E. A., and Bruckner, A. P., "High-Resolution Measurements of Ram Accelerator Gasdynamic Phenomena," AIAA Paper 92-3244, July 1992.

[34]Knowlen, C., and Sasoh, A., "Ram Accelerator Performance Modeling," *Ram Accelerators,* Springer-Verlag, 1998, Heidelberg, Germany, pp. 25–37.

[35]Knowlen, C., and Bruckner, A. P., "Experimental Correlation of Ram Accelerator Hugoniot Theory," French–German Research Inst. of Saint-Louis, Saint-Louis, France, Paper 14, 1993.

[36]Sasoh, A., and Knowlen, C., "Ram Accelerator Operation Analysis in Thermally Choked and Transdetonative Propulsive Modes," *Transactions of the Japan Society for Aeronautical and Space Sciences*, Vol. 40, No. 128, 1997, pp. 130–148.